X-734-70-50
PREPRINT

EJECTION OF INTERNAL MASS FROM SPINNING SPACECRAFT WITH COLLISION INTERACTIONS

FRANZ ZACH

JANUARY 1970

GODDARD SPACE FLIGHT CENTER
GREENBELT, MARYLAND

X-734-70-50

PREPRINT

EJECTION OF INTERNAL MASS FRCM SPINNING SPACECRAFT WITH COLLISION INTERACTIONS

Franz Zach

January 1970

Goddard Space Flight Center

Greenbelt, Maryland

CONTENTS

EJECTION OF INTERNAL MASS FROM SPINNING SPACECRAFT WITH COLLISION INTERACTIONS

Franz Zach

ABSTRACT*

This report treats ejection of internally stored mass (e.g. an apogee motor casing) from a spinning spacecraft wherein a collision occurs. The problem is attacked by formulation of two processes: first, an ejection process which includes the release mechanism, the separation trajectory of stored mass relative to spacecraft, and the determination of the collision point; and second a collision process wherein the impulse exchanged is computed based upon consideration of surface friction, mechanical deformations, and coefficient of restitution. A specific case is treated where both direction and magnitude of spacecraft body rates following collision are determined as functions of the collision parameters. A knowledge of these body rates is required to perform directional despin of a spacecraft about its final axis of maximum moment of inertia.

---

*The work for this paper was performed while the author was granted a National Research Council Postdoctoral Resident Research Associateship supported by the NASA/Goddard Space Flight Center. The author is very much indebted to Mr. W. Isley, Mr. E. Stengard, Mr. R. Bartlett and Mr. D. Endres for their contributions.

Nomenclature and Abbreviations

a	distance from CMS to CMC
B_1, B_2	brackets of the solar aspect sensor
b	distance from CMM to CMC
CMC	center of mass of spacecraft and internal mass together, before ejection of internal mass
CMM	center of mass of internal mass alone
CMS	center of mass of spacecraft alone
$\vec{D}$	angular momentum
E_d	energy transferred from motion into deformation
e	coefficient of restitution
$\vec{e}_x, \vec{e}_y, \vec{e}_z$	unity vectors in directions x, y or z respectively
f	range of spring operation
$\vec{I}$	impulse
[I]	moment of inertia matrix
I_{max}	maximum moment of inertia
M	motor
m_M	mass of the internal mass alone
m_S	mass of the spacecraft alone
$\vec{n}$	unity vector normal to collision surface
P	point of collision on the spacecraft measured in the x_S, y_S, z_S set
Q	point of collision on the motor measures in the x_M, y_M, z_M set
$\vec{r}$	distance vector
$\vec{r}_S$	distance vector from CMS to P
$\vec{r}_M$	distance vector from CMM to P

$\vec{S}$	spacecraft
$\vec{S}$	collision vector
SAS	solar aspect sensor
SM_1	spin mode before deployment of internal mass
SM_2	spin mode after deployment of internal mass
t	time
$\vec{v}$	velocity
$\vec{v}_M$	velocity of CMM
$\vec{v}_{MP}$	velocity of colliding point of motor
$\vec{v}_S$	velocity of CMS
$\vec{v}_{SP}$	velocity of colliding point of spacecraft
x,y,z	right handed coordinate system with center in CMC and axes along axes of principal moments of inertia
x_S, y_S, z_S	right handed coordinate system with center in CMS and axes parallel to the x, y, z set
x_M, y_M, z_M	right handed coordinate system with center in CMM and axes parallel to the x, y, z set
μ	coefficient of friction
ζ, η, ξ	inertial coordinate system
ζ^*, η^*, ξ^*	coordinate system with center in CMM and axes parallel to ζ, η, ξ
ρ	angle of friction, = $\arctan \mu$
σ	angle of $\vec{S}$ against -y
$\vec{\omega}$	vector of angular velocity

EJECTION OF INTERNAL MASS FROM SPINNING SPACECRAFT WITH COLLISION INTERACTIONS

1. INTRODUCTION

A spacecraft despin maneuver is often required following orbit injection and deployment of the apogee motor casing. This report treats ejection of such stored mass under conditions where the spin axis after apogee motor burnout is not the spacecraft axis of maximum inertia. This condition could result from a damping mechanism which is not compensated for by active nutation control.

Under such circumstances, the spin axis will now be aligned along the new axis of maximum inertia which will not be the axis of symmetry, normally assumed for motor ejection. This can produce a collision process between the ejected mass and spacecraft, wherein the resulting body rates can dictate the final spin direction. The determination of body rates can be approached through definition of an Ejection Process and a Collision Process. In the Ejection Process, the release mechanism, departure trajectory and collision point are established. This is then followed by formulation of the Collision Process wherein impulse exchange is computed in terms of surface friction effects, mechanical deformations, and coefficient of restitution. Based upon the impulse exchange, direction and magnitude of spacecraft body rates are determined. Some despin mechanisms, such as Yo-Yo devices , require a specified initial spin direction in order to remove angular momentum. If the axis of deployment symmetry becomes the axis of maximum inertia following motion ejection, then final spin direction will be determined by direction and magnitude of body rates after collision and damping characteristics of the spacecraft structure.

It is therefore apparent that estimation of body rates after collision can dictate ultimate despin capability of the spacecraft. Part 2 develops equations for the Ejection Process. The release mechanism is modeled in Section 2.1 as an impulsive device, which essentially idealizes the acceleration as a pure addition of velocity.

In Section 2.2 the release mechanism is defined to represent time dependent acceleration. In Section 2.3, Collision point and closing velocity are determined. Part 3 treats the collision process. Section 3.1 considers a representative static structural load test. The collision impulse vector ($\vec{S}$) is computed as a result of much test data. In Section 3.2 a mathematical model is developed for calculation of $\vec{S}$. This Section also covers determination of body rates due to the collision process which are evaluated as functions of coefficient of restitution and surface friction.

2. The Ejection Process – Trajectory and Collision Point

2.1 Release Mechanism – Impulsive

Figure 1 shows an example of the geometric configuration for the spacecraft and stored mass which is represented herein as an apogee motor casing. It shall be assumed, that the x-axis is the axis of maximum moment of inertia and that spin is stabilized about this axis. This fact is indicated by ω_x in Fig. 1. It shall be assumed further that the apogee motor is released during this rotation and accelerated by springs in the z-direction. The springs usually are effective only over a small distance and are located rotational-symmetric about the z-axis. It is assumed herein that the release mechanism involves no tip-off errors. This means that there are no reaction torques between spacecraft and

apogee motor due to separation, and implies that no change of angular velocity is produced during separation. Therefore, both spacecraft following separation and apogee motor casing will have the same $\vec{\omega}$ as the original composite spacecraft. The fact that the springs usually work only over a small distance results in a simplification of the problem: The motion of spacecraft and apogee motor can be calculated under the assumption that the springs impart a relative velocity in z-direction to spacecraft and apogee motor in an impulsive manner.

Figure 2 shows the situation immediately after release. The relative velocity in z-direction is given by the experimental data for the spring force and shall be called v_{rz}:

$$v_{rz} = |v_{Mz}| + |v_{Sz}|. \tag{1}$$

Because there are no other forces active, the law of conservation of impulse yields

$$m_M |v_{Mz}| - m_S |v_{Sz}| = 0, \tag{2}$$

which together with (1) allows calculation of $|v_{Mz}|$ and $|v_{Sz}|$. v_{My} and v_{Sy} are obtained as follows: upon separation, the CMM rotates through displacement b about CMC with the angular velocity ω_x, CMS rotates about CMC with ω_x through displacement a (see Figs. 1 and 2). Because there are no impulses in y-direction due to separation, the motor will move with velocity:

$$v_{My} = -\omega_x b \tag{3}$$

and the spacecraft will move with velocity

$$v_{Sy} = \omega_x a \tag{4}$$

As some time t after deployment, relative position and motion in an inertial coordinate system will be as shown in Fig. 3. The displacements are given by:

$$\left.\begin{aligned} \eta_M^* (t) &= \eta_M(t) - \eta_S(t) \\ \zeta_M^* (t) &= \zeta_M(t) - \zeta_S(t) \end{aligned}\right\} \tag{5}$$

and

$$\left.\begin{aligned} y (t) &= - \zeta^* (t) \sin \omega t + \eta^* (t) \cos \omega t \\ z (t) &= \zeta^* (t) \cos \omega t + \eta^* (t) \sin \omega t \end{aligned}\right\} \tag{6}$$

y(t) and z(t) give the motion of the apogee motor with respect to the CMS.

Based on Figs. (1) through (3), displacements in the η, ζ coordinate systems become:

$$\left.\begin{aligned} \eta_M(t) &= v_{My}\, t = |\omega_x|\, bt, \\ \zeta_M(t) &= v_{Mz}\, t + b, \\ \eta_S(t) &= v_{Sy}\, t = - |\omega_x|\, at, \\ \zeta_S(t) &= v_{Sz}\, t - a = - v_{Mz} \frac{m_M}{m_S}\, t - a, \end{aligned}\right\} \tag{7}$$

and

$$\left.\begin{aligned} \eta_M^*(t) &= (a + b)\, |\omega_x|\, t \\ \zeta_M^*(t) &= v_{Mz} \left(1 + \frac{m_M}{m_S}\right) t + a + b = v_{rz}\, t + a + b. \end{aligned}\right\} \tag{8}$$

Entering Eq. (8) into Eq. (6) now gives the time history of the CMM in the y-z coordinate system. Because the same ω_x is valid for spacecraft and motor after deployment, Eq. (6) produces the trajectory of every part of the motor with respect to the spacecraft, the initial condition being given by Fig. 2. The

axes of rotational symmetry (aligned along the z-axis in Fig. 2) of spacecraft and apogee motor always remain parallel.

Figure 4 shows trajectories based upon the following values:

$$\left.\begin{aligned} &a = 3.2'',\ b = 26.24'' \\ &\omega_x = -10 \text{ rpm to } -150 \text{ rpm} \\ &v_{rz} = 41.9 \text{ in/sec.} \end{aligned}\right\} \tag{9}$$

Calculations with varying ω_x and $v_{rz} = 0$ produce trajectories which fall on top of the case where $\omega_x = -150$ rmp in Fig. 4. This shows the spring to have little effect on the trajectory for ω_x greater than 92 rpm.

2.2 Release Mechanism - Time Dependent Acceleration

The previous section considered the release mechanism to be impulsive. For time dependent acceleration consider Fig. 5 and assume at first deployment without a spring. The deployment is assumed to be in the instant when the z-axis passes through the ζ' -axis. The $\eta' - \zeta'$ system has its origin in CMS, the η' axis is not rotating and points in the z-direction in the instant of release.

Defining r(t) in terms of Eq. (8) gives

$$r(t) = \sqrt{\eta_M^{*2}(t) + \zeta_M^{*2}(t)} = (a + b)\sqrt{1 + (\omega_x t)^2} \tag{10}$$

and

$$\ddot{r}(t) = (a + b)\,\omega_x^2\,(1 + \omega_x^2\,t^2)^{-3/2}. \tag{11}$$

For the additional acceleration caused by the spring the force F is:

$$F = K\,[r - (a + b)]$$

where K is the spring constant.

The acceleration of the apogee motor due to the spring is F/m_M and the acceleration of the spacecraft is F/m_S.

The sum of these accelerations gives $\ddot{r}(t)$ due to the spring. The validity of this calculation is over the range f of spring-operation.

Entering the additional acceleration into Eq. (11) gives

$$\left.\begin{aligned} \ddot{r}(t) = (a+b)\,\omega_x^2\,(1+\omega_x^2 t)^{-3/2} + K\,\frac{m_M + m_S}{m_M m_S}\,[r - (a+b)] \\ \text{for } a+b \le r \le a+b+f. \end{aligned}\right\} \tag{12}$$

Consider a specific case having the following parameter values:

$$\left.\begin{aligned} \omega_x &= -92 \text{ rpm} \\ K &= 2.81 \times 10^6 \text{ slg } s^{-2} \\ f &= 1'' \\ a+b &= 29.44'' \end{aligned}\right\} \tag{13}$$

Calculations of the two extremes, i.e.

(a) no spring at all

(b) spring action executed impulsively

show approximately no difference in the trajectories. Eq. (12) gains importance for higher spring forces and lower $|\omega_x|$.

2.3 Collision Point and Closing Velocity

The trajectory of the CMM has been developed in Sections 2.1 and 2.2. The determination of initial collision point must be based upon the surface configuration of motor and spacecraft.

In Fig. 6 $Q_i(x, y, z)$ represents any selected point on the motor surface and $P_i(x, y, z)$ a corresponding point of intersection with the spacecraft surface as determined by transformation of the CMM trajectory into $Q_i(x, y, z)$. The

initial collision is found by solving the minimum time problem for all permissible $Q_i(x, y, z)$ mapped into the set of all points P_i (x, y, z).

A geometrical solution is most often the simplest means of finding the initial collision point where surface envelopes are matched in a graphical manner.

The solution for the initial collision point shall be designated $P = P(x_S, y_S, z_S)$ on the spacecraft and Q (x_M, y_M, z_M) on the motor.

x_S, y_S, z_S coordinates are measured with respect to CMS. The x_M, y_M, z_M are coordinates measured with respect to CMM· Consider a configuration which yields a collision point characterized by P = (-3.9, - 22.5, 32.9) and Q = (-4.8, -16.1, -6.3). The time to collision at point P is obtained by solving Eqs. (6) and (8) for t with

$$y(t) = \Delta y = y_S - y_M$$

and

$$z(t) = \Delta z = z_S - (a + b + z_M).$$

The closing velocity components can be obtained by differentiation of Eqs. (6) and (8) with respect to time. Using the following values:

$$y_S = - 22.5''$$
$$z_S = \ \ 32.9''$$
$$y_M = - 16.1''$$
$$z_M = - \ \ 6.3''$$

the closing velocity components are found to be:

$$v_{yr} = -171 \text{ in/sec}$$

and

$$v_{zr} = 164 \text{ in/sec.}$$

3. Collision Process

Once it has been established that a collision takes place using methods described in Section 2.3, it becomes necessary to formulate a dynamics model for the collision process.

It is important to calculate the impulse exchange between internal mass and spacecraft which gives the initial condition of translatory and rotational velocity after collision.

For this purpose a good approach is to assume a collision vector $\vec{S}$ (Ref. 1) which is the time-integral over the forces in action during collision:

$$\vec{S} = \int_0^t \vec{F}\, dt. \tag{14}$$

$\vec{F}$ as a function of time is given by the geometry at the collision point, by the amount of the relative velocity, by the masses of the colliding bodies and the structural properties of the two bodies in the area which is effected by the collision.

For the purpose of evaluating a specific collision process, it is assumed that the motor and spacecraft configurations at the instant of collision are as represented in Fig. 7. The impact geometry shows initial contact with a bracket (B_1) which supports a solar aspect sensor at 12° angle measured from minus y. The second impact takes place at bracket (B_2) at 30° angle.

3.1 Collision Vector Determined From Static Structural Data

Assume that static measurements have been performed for simultaneous loading of two brackets of the type shown in Fig. 7 and that deformation behavior is as represented in Fig. 8. From Fig. 7 geometry, bracket B_2 will not be contacted until bracket B_1 has deformed .625". Let $t = 0$ denote the time when B_1 deformation is initiated, $t = t_1$ the time when B_2 deformation is initiated, and $t = t_2$ the end of deformation. The time t_2 is also the moment when the entire kinetic energy, present at $t = 0$, is absorbed by the deformed material. Fig. 9 gives the deformation diagram for both brackets with the time history outlined above, where t_2 occurs when the area under the deflection curve for $B_1 + B_2$ equals to the initial kinetic energy.

Using the value of v_{yr} taken from Section 2.3, the kinetic energy to be absorbed by the structure is:

$$T = 4618 \text{ lb in.} \tag{15}$$

The kinetic energy absorbed at t_1 can be taken from Fig. 9 as 230 lb-in. Therefore, 4388 lb-in., are to be absorbed when both brackets are deformed simultaneously. It should be noted that the deformation of the first bracket is already in a more advanced phase than the deformation of the second bracket.

Considering Eq. (14) for $\vec{S}$ the direction and magnitude of $\vec{F}$ has to be given at all times. The magnitude is given by Fig. 9, the direction by the surface at the collision point, and the friction coefficient μ. This latter term gives the maximum angle of deviation of actual force acting between the two bodies from normal to surface at collision interaction. There is always some

uncertainty in predicting the surface configuration due to (1) reproducibility of test data and (2) proper modeling of the structural dynamics. However, in this case a good assumption can be made by knowing that the surface of the motor at the collision point is highly rigid whereas the brackets are deformed very easily. The collision surface therefore is given primarily by the shape of the motor. Considering Fig. 7 shows a deviation of 12° from a plane normal to y during deformation of B_1. For deformation of brackets B_1 and B_2 both are considered separately, therefore giving the same 12° as above for B_1 and 30° for B_2. $\vec{F}_1$ will be called the force acting on B_1, $\vec{F}_2$ the force acting on B_2.

According to Eq. (14) we receive with

$$v_{yr} = \frac{ds_y}{dt} = v(s)$$

where s_y is the deflection taken from Fig. 9:

$$\vec{S} = \int \vec{F}\, dt = \int \vec{F}\, \frac{ds_y}{v_{yr}} \quad , \tag{16}$$

where v_{yr} can be calculated as follows: the kinetic energy at t = 0 is given by

$$T_y\,(0) = \frac{1}{2}\, m_M\, v_{yr}^2\,(0) \tag{17}$$

and will be reduced due to the area E_d under the curve in Fig. 9:

$$T_y(0) - T_y(t) = E_d. \tag{18}$$

With

$$T_y(t) = \frac{1}{2} m_M v_{yr}^2(t) \tag{19}$$

we receive

$$v_{yr}(t) = \sqrt{v_{yr}^2(0) - \frac{2}{m_M} E_d} \tag{20}$$

which is given in Fig. 10.

Determination of the direction of $\vec{F}$ in every moment involves the following considerations: with very high friction the force would be aligned along y, because this is the direction of impact. With small friction deviation of the direction of the force from normal to collision surface cannot be different more than given by μ.

The normal to the impact surface at B_1 is 12° and at B_2 is 30° off from y-direction. If we assume that the bracket is made of aluminum, the motor of steel, and the contact surface is lubricated, μ will range from .1 to .2.

Then, $\vec{F}_2$ will deviate from the y-direction by 24.3° for μ = .1, and 18.7° for μ = .2.

Eq. (16) can be written in the form

$$\vec{S} = \int_{s(0)}^{s(t_1)} \frac{\vec{F}}{v} ds + \int_{s(t_1)}^{s(t_2)} \frac{\vec{F}}{v} ds = \int_{s(0)}^{s(t_2)} \frac{\vec{F}_1}{v} ds + \int_{s(t_1)}^{s(t_2)} \frac{\vec{F}_2}{v} ds \tag{21}$$

since $\vec{F}_2$ is $\neq 0$ only for $t_1 \leq t < t_2$. Figure 11 now shows F/v for B_1 and for B_2, both as a function of the deflection, s.

The area under the graphs in Fig. 11 now gives the absolute value of $\vec{S}$ for B_1 and B_2. However, it must be noted that this is only valid for an inelastic collision process, where no forces are acting between the two bodies after the maximum deformation of the structure is obtained.

(The direction of $\vec{S}$ for B_1 and B_2 is given by the normal to the collision surface at B_1 or B_2 respectively and by μ).

The area under the graphs in Fig. 11 can be determined graphically from s = 0 to s = 2.1". F_1/v and F_2/v reach infinity at s = 2.17"; therefore, from s = 2.1" to s = 2.17" an analytic form of integration must be applied.

F_1 and F_2 constitute the numerator for F_1/v and F_2/v and only the interval $2.1" \leq s \leq 2.17"$ is considered F_1 and F_2 can be treated as constants for the purpose of integration.

For v(s), Eq. (20) can be applied where the term $-2E_d/m_M$ can be expressed in terms of s. This can be done by graphic approximation of E_d in Fig. 10: from s = 1.75" to 2.5" E_d can be approximated by the linear expression:

$$E_d = \frac{2}{m_M} (k_2 s - k_1). \tag{22}$$

Evaluating k_1 and k_2 from E_d in Fig. 10 and substituting in Eq. (20) yields:

$$v = v_0 \sqrt{2.36 - 1.09 s}. \tag{23}$$

Integration in Fig. 11 now results in:

and

$$\left.\begin{aligned} |\vec{S}_1| &= 37.6 \text{ lb-sec} \\ |\vec{S}_2| &= 16.7 \text{ lb-sec.} \end{aligned}\right\} \tag{24}$$

We are interested mainly in the further motion of the spacecraft, namely ω_z immediately after collision. For this purpose the change of angular momentum shall be calculated based upon

$$\Delta\vec{D} = \int_0^{t_2} \vec{r} \times \vec{F}\, dt \tag{25}$$

where $0 \leq t \leq t_2$ is the time interval during which the collision happens, and generally is assumed to be very short. $\vec{r}$ is a vector leading from the CMS to a point where $\vec{F}$ is acting. Here, two points of collision must be considered with $\vec{r}_1$ leading to B_1 and $\vec{r}_2$ leading to B_2, where $\vec{r}_1$ and $\vec{r}_2$ are assumed to remain constant during $0 \leq t \leq t_2$. Therefore, Eq. (25) can be written as:

$$\Delta\vec{D} = \vec{r}_1 \times \int_0^{t_2} \vec{F}_1\, dt + \vec{r}_2 \times \int_0^{t_2} \vec{F}_2\, dt = \vec{r}_1 \times \vec{S}_1 + \vec{r}_2 \times \vec{S}_2 .$$

Using Fig. 7, $\vec{r}_1$, $\vec{r}_2$, $\vec{S}_1$ and $\vec{S}_2$ can be determined as shown in Fig. 12. The collision point can be represented by:

and

$$\left.\begin{aligned} \vec{r}_1 &= -3.5\,\vec{e}_x - 21.9\,\vec{e}_y + 32.9\,\vec{e}_z \\ \vec{r}_2 &= -8.4\,\vec{e}_x - 20\,\vec{e}_y + 32.9\,\vec{e}_z . \end{aligned}\right\} \tag{26}$$

Using Fig. 5 it can be determined that a collision takes place when the trajectory of the motor forms an angle of 45° with the z-axis. Therefore, the following expression for components of the collision vector is valid:

$$S_{iz} = \sqrt{S_{ix}^2 + S_{iy}^2} \quad \text{for } i = 1, 2. \tag{27}$$

Now the following expressions can be written with $\rho = \arctan \mu$

$$\left.\begin{aligned}
&\vec{S}_1 = -37.6 \sin (12° - \rho)\, \vec{e}_x - 37.6 \cos (12° - \rho)\, \vec{e}_y + 37.6\, \vec{e}_z \text{ for } 0 \le \rho \le 12°, \\
&\vec{S}_1 = -37.6\, \vec{e}_y + 37.6\, \vec{e}_z \text{ for } \rho \ge 12°, \\
&\vec{S}_2 = -16.7 \sin (30° - \rho)\, \vec{e}_x - 16.7 \cos (30° - \rho)\, \vec{e}_y + 16.7\, \vec{e}_z \text{ for } 0 \le \rho \le 30°
\end{aligned}\right\} \quad (28)$$

and

$$\vec{S}_2 = -16.7\, \vec{e}_y + 16.7\, \vec{e}_z \text{ for } \rho \ge 30°.$$

We are mainly interested in changes of angular velocity ΔD_s of the spacecraft about its z-axis. Combination of Eqs. (25), (26), and (28) yields:

$$\Delta D_{zs} = \sum_{i=1}^{2} (r_{x_i} F_{y_i} - r_{y_i} F_{x_i}). \qquad \text{(a)}$$

This leads to

$$\left.\begin{aligned}
&\Delta D_{zs} = 1161.5 \sin \rho - 164 \cos \rho \text{ for } 0 \le \rho \le 12°, && \text{(b)} \\
&\Delta D_{zs} = 90 + 339 \sin \rho - 80 \cos \rho \text{ for } 12° \le \rho \le 30° && \text{(c)}
\end{aligned}\right\} \quad (29)$$

and

$$\Delta D_{zs} = 190 \text{ for } \rho \ge 30°. \qquad \text{(d)}$$

The above mentioned uncertainties in surface configuration can be put into Eqs. (25) through (29). For example, the uncertainty in μ can be considered by changing ρ in Eq. (29) to smaller and greater values starting from the most likely value of ρ. It can be calculated from Eq. (29b) that

$$\left.\begin{aligned} &\Delta D_{zz} \leq 0 \text{ for } \mu = tg\rho \leq .142 \\ \text{and} \quad &\Delta D_{zz} \geq 0 \text{ for } \mu = tg\rho \geq .142 \end{aligned}\right\} \tag{30}$$

If a positive value of ω_{zz} after collision is desired, $\mu = .142$ gives the lower limit for friction between the colliding surfaces.

As pointed out earlier, the above calculations of $|\vec{S}|$ by integration of the areas in Fig. 11 are made under the assumption of inelastic collision. To consider different degrees of elasticity a different approach is applied as follows.

3.2 Collision Process Based Upon Coefficient of Restitution

In this section we apply another approach for calculating the collision vectors $\vec{S}_1$ and $\vec{S}_2$. For simplification, $\vec{S}_1$ and $\vec{S}_2$ are combined to one vector $\vec{S}$. $\vec{S}$ can be calculated directly based upon the dynamics of the collision when a coefficient of restitution is assumed. The coefficient of restitution gives the degree of elasticity involved in a collision process. The coefficient of restitution e (Ref. 2) is defined as

$$e = \frac{v_S' - v_M'}{v_M - v_S}, \tag{31}$$

where v_M and v_S are the velocities normal to the collision surface before collision of motor or spacecraft, respectively, and v_M' and v_S' are these values after collision. Generally, all prime terms represent values after collision. All velocities have to be taken at the point of collision and are different in general from the velocities of CMS and CMM.

e = 0 denotes a completely inelastic collision,

e = 1 a completely elastic collision.

In order to receive the change in motion due to collision, we relate the inputs and the angular momentum of both the spacecraft and the apogee motor to the collision vector.

$$\left.\begin{aligned} \vec{I}_S' - \vec{I}_S &= \vec{S} \\ \vec{I}_M' - \vec{I}_M &= -\vec{S} \\ \vec{D}_S' - \vec{D}_S &= \vec{r}_S \times \vec{S} \\ \vec{D}_M' - \vec{D}_M &= \vec{r}_M \times (-\vec{S}) \end{aligned}\right\} \qquad (32)$$

$\vec{r}_s$ is the distance vector from CMS to the point of collision P, $\vec{r}_M$ is the distance vector from CMM to P. Consider only the change of motion due to collision and set $\vec{I}_S = 0$, $\vec{D}_M = \vec{D}_S = 0$.

Eq. (32) can be written as:

$$\left.\begin{aligned} m_S \vec{v}_S' &= \vec{S}, \\ m_M (\vec{v}_M' - \vec{v}_M) &= -\vec{S}, \\ [I_S]\, \omega_S' &= \vec{r}_S \times \vec{S} \\ [I_M]\, \vec{\omega}_S' &= -\vec{r}_M \times \vec{S}. \end{aligned}\right\} \qquad (33)$$

and

The velocity immediately before collision is $\vec{v}_{MP} = \vec{v}_M$, and $\vec{v}_S = \vec{v}_{SP} = 0$.

The velocities immediately after collision are:

$$\vec{v}'_{SP} = \vec{v}'_S + [I_S]^{-1} [\vec{r}_S \times \vec{S}] \times \vec{r}_S$$

and (34)

$$\vec{v}'_{MP} = \vec{v}'_M + [I_M]^{-1} [\vec{r}_M \times (-\vec{S})] \times \vec{r}_M .$$

With $\vec{n}$ denoting the unity vector normal to the collision surface, Eq. (31) can be written as follows:

$$\{v'_S + [[I_S]^{-1} (\vec{r}_S \times \vec{S})] \times \vec{r}'_S - \vec{v}'_M - [[I_M]^{-1} (\vec{r}_M \times (\vec{S}))] \times \vec{r}_M \} \cdot \{\vec{n}\} = e \{\vec{v}_M\} \cdot \{\vec{n}\} \quad (35)$$

($\times$ denotes a cross product, $\cdot$ a dot product).

Instead of assuming two different collision points (P_1 and P_2 in Fig. 12) we assume the collision impulse acting at a point P between P_1 and P_2. $\vec{S}$ is now determined by its magnitude $|S|$ and angle σ against the minus y-axis. The amount $|\vec{S}|$, can be calculated from Eq. (35) by assuming e. It is found that for assuming full inelasticity $|S|$ based on this calculation is equal to $|\vec{S}_1 + \vec{S}_2|$ as calculated in Section 3.1. The angle σ is determined herein on the basis of an inelastic collision process, where it has been tacitly assumed that $\vec{S}$ produces the same resulting D_{sz} as in Section 3.1. This condition results in Fig. 13 where Eq. (29) is applied and compared with

$$\Delta \vec{D} = \vec{r}_S \times \vec{S}, \quad (36)$$

where

$$\vec{r}_S = -3.9\,\vec{e}_x - 22.5\,\vec{e}_y + 32.9\,\vec{e}_z \tag{37}$$

is assumed as distance from CMS to P.

Based upon σ taken from Fig. 13 and the condition according to Eq. (27) $\vec{S}$ can be expressed by:

$$\left.\begin{aligned} \vec{S} &= -\frac{S}{\sqrt{2}}\sin\sigma\,\vec{e}_x - \frac{S}{\sqrt{2}}\cos\sigma\,\vec{e}_y + \frac{S}{\sqrt{2}}\,\vec{e}_z, \\ &\text{where} \\ S &= |\vec{S}|. \end{aligned}\right\} \tag{38}$$

The structure is deformed continuously during collision. It is reasonable to assume that deformation is such that $\vec{n}$, (which is necessary for application of Eq. (31)) lies approximately in the direction of $\vec{S}$.

Therefore, Eq. (38) can be written as

$$\vec{S} = S\,\vec{n} \tag{39}$$

and

$$\vec{n} = -\frac{\sin\sigma}{\sqrt{2}}\,\vec{e}_x - \frac{\cos\sigma}{\sqrt{2}}\,\vec{e}_y + \frac{1}{\sqrt{2}}\,\vec{e}_z. \tag{40}$$

This flexibility in considering structural deformation at the point of collision is an advantage of this approach compared to that used in section 3.1.

Eqs. (33) and (39) now are inserted into Eq. (35) in order to receive the following equation for $|S|$:

$$|S| = \frac{(e+1)\,\vec{n}\cdot\vec{v}_M}{\left\{\frac{1}{m_S}\vec{n} + [[I_S]^{-1}(\vec{r}_S\times\vec{n})]\times\vec{r}_S - \frac{1}{m_M}\vec{n} - [[I_M]^{-1}[\vec{r}_M\times(-\vec{n})]]\times\vec{r}_M\right\}\cdot\{\vec{n}\}} \tag{41}$$

$\vec{S}$ now can be inserted into Eq. (33) and the motion of spacecraft and motor after collision can be calculated.

For this purpose the following special values for masses and moments of inertia are chosen:

a. for the spacecraft and apogee-motor combined

M_c = 1125 lbs.

I_{cxx} = 115.6 slg ft^2

I_{cyy} = 111.9 slg ft^2

I_{czz} = 105.9 slg ft^2

b. for the spacecraft alone

M_S = 1003 lbs

I_{Sxx} = 87.7 slg ft^2

I_{Syy} = 84.0 slg ft^2

I_{Szz} = 101.17 slg ft^2

c. for the apogee-motor casing alone

M_M = 122 lbs.

I_{Mxx} = 7.35 slg ft^2

I_{Myy} = 7.35 slg ft^2

I_{Mzz} = 4.33 slg ft^2

$\vec{r}_S$ is given by Eq. (37)

$\vec{r}_M$ = $-4.8\ \vec{e}_x - 16.1\ \vec{e}_y + 6.3\ \vec{e}_z$

Figs. 14a and 14b show the change in ω_x, ω_y and ω_z for the spacecraft as function of σ and e. The value of σ, where ω_z changes its sign is called $\sigma_{critical}$ The corresponding value for μ can be found to be $\mu_{critical} = .141$. Lower frictions than $\mu_{critical}$ give negative ω_z contributions to the motions of the spacecraft after deployment of the apogee motor.

4. Discussion of Results

Equations developed in Sections 2 and 3 can be used to establish ejection and collision processes if the following parameters can be specified:

1. Moments of inertia for spacecraft and ejected body
2. Mass of spacecraft and ejected body
3. Geometrical configuration for C.M. locations in spacecraft and ejected body
4. Surface friction properties at impact point
5. Structural elastic properties at impact point (expressed in terms of coefficient of restitution)
6. Release mechanism behavior
7. Velocities and angular rates prior to release
8. Impact geometry and deformation time-history

Usually, parameters (1), (2), (3) and (6) are readily available for a given spacecraft. Parameter (7) can be established by in-flight measurement. The uncertainties associated with these items are considered herein to be small and would have no significant influence upon the impact study. However, parameters (4), (5) and (8) are generally not known to such precision and must be treated within a bound of uncertainty in order to predict limits of impact behavior. For example, both surface friction and elastic properties are normally

based upon practical tests wherein reproducibility of data is of prime concern. The uncertainties associated with these parameters can be used to determine a range of collision vectors, $\vec{S}$, which then permits a prediction of the upper and lower bounds on resulting body rates following impact.

Consider now the special case described in Sections 2 and 3 where parameter (8) is based upon static test data. The influence of parameters (4) and (5) is shown in Figures 14a and 14b. The friction coefficient for a lubricated surface of the selected materials is estimated to lie at a value between 0.1 and 0.15. The angle sigma can be used to set upper and lower bounds of uncertainty on the friction coefficient. The upper bound on sigma is 17.5 degrees, which results from the consideration that friction coefficient becomes zero at this angle. The lower bound on sigma is 0 degrees and represents the point where friction coefficient exceeds a value of 0.577. This limiting value is based upon the angles shown in Figure 7, wherein tan 30° equals 0.577. A range of values for coefficient of restitution, e, from 0 (inelastic case) to 0.5 was considered for the structural elastic behavior. Higher values for e are not likely to occur for the subject case. Figure 14b shows that e has no effect upon determination of direction for ω_z. For the most likely condition of inelastic collision, ω_z is found to range from +0.12 radians per second (6.87 degrees per second) at friction factors of 0.577 and above to - 0.10 radians per second (-5.73 degrees per second) at zero friction. Where no lubrication is applied to the contact surfaces, one can expect the friction coefficient for bare metal surfaces to be unity or higher. If the surfaces are painted, one could expect even higher friction factors. Either of these latter two conditions would produce an ω_z of about +0.1 radians per second. It is of interest to note that the lubricated condition will produce an ω_z having bounds of +0.01 radians per second and -0.028 radians per second.

5. Conclusions

A semi-analytic approach has been developed herein for determining the residual spacecraft body rates produced by impact with an ejected mass. Two processes are involved. The first phase describes the mass ejection, which is handled analytically. The second phase is the collision process which requires formulation of an empirical deformation model which is combined with an analytic model for the collision vector.

A specific case, examined using this mathematical approach, revealed that the residual spacecraft z axis rate can be bounded by coefficient of restitution and surface friction properties. The coefficient of restitution influences only the magnitude of the residual rate whereas the direction is given by surface friction.

List of Illustrations

Fig. 14b. Changes of ω_z as a function of σ (and therefore as a function of μ according to Fig. 12). The parameter is the coefficient of restitution which gives the degree of elasticity involved.

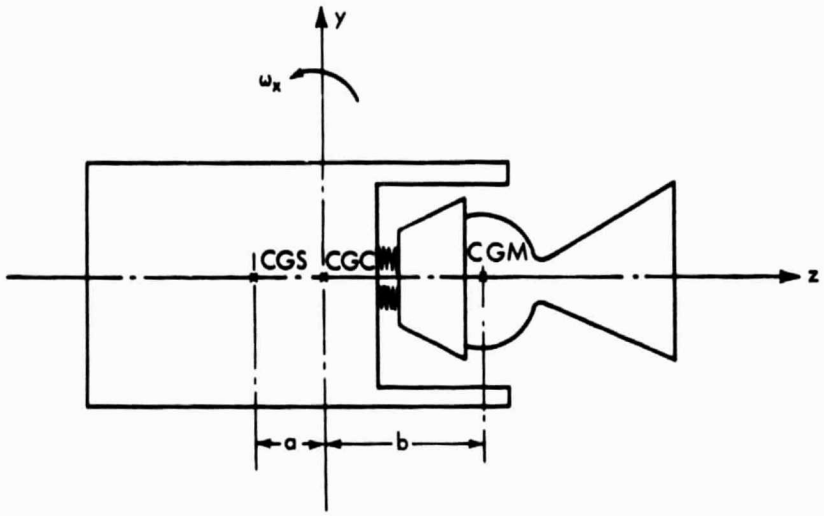

Figure 1. Geometric configuration of the spacecraft and the internal mass, (i.e. apogee motor).

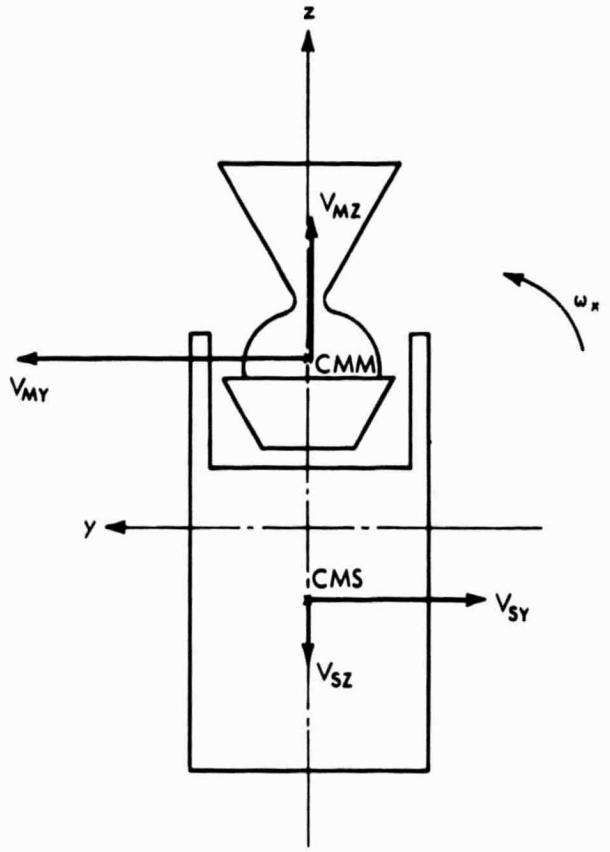

Figure 2. Velocities of the spacecraft and the apogee motor in the moment after release.

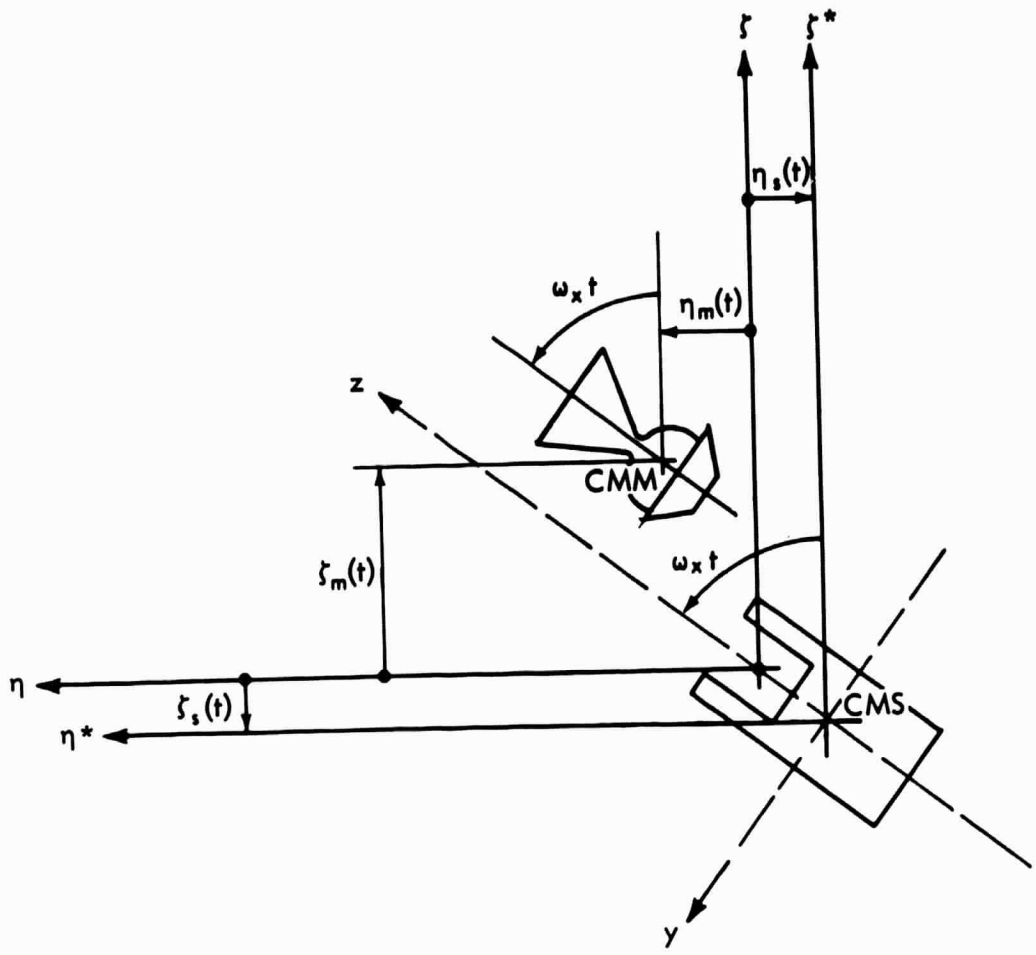

Figure 3. Location of spacecraft and motor after deployment.

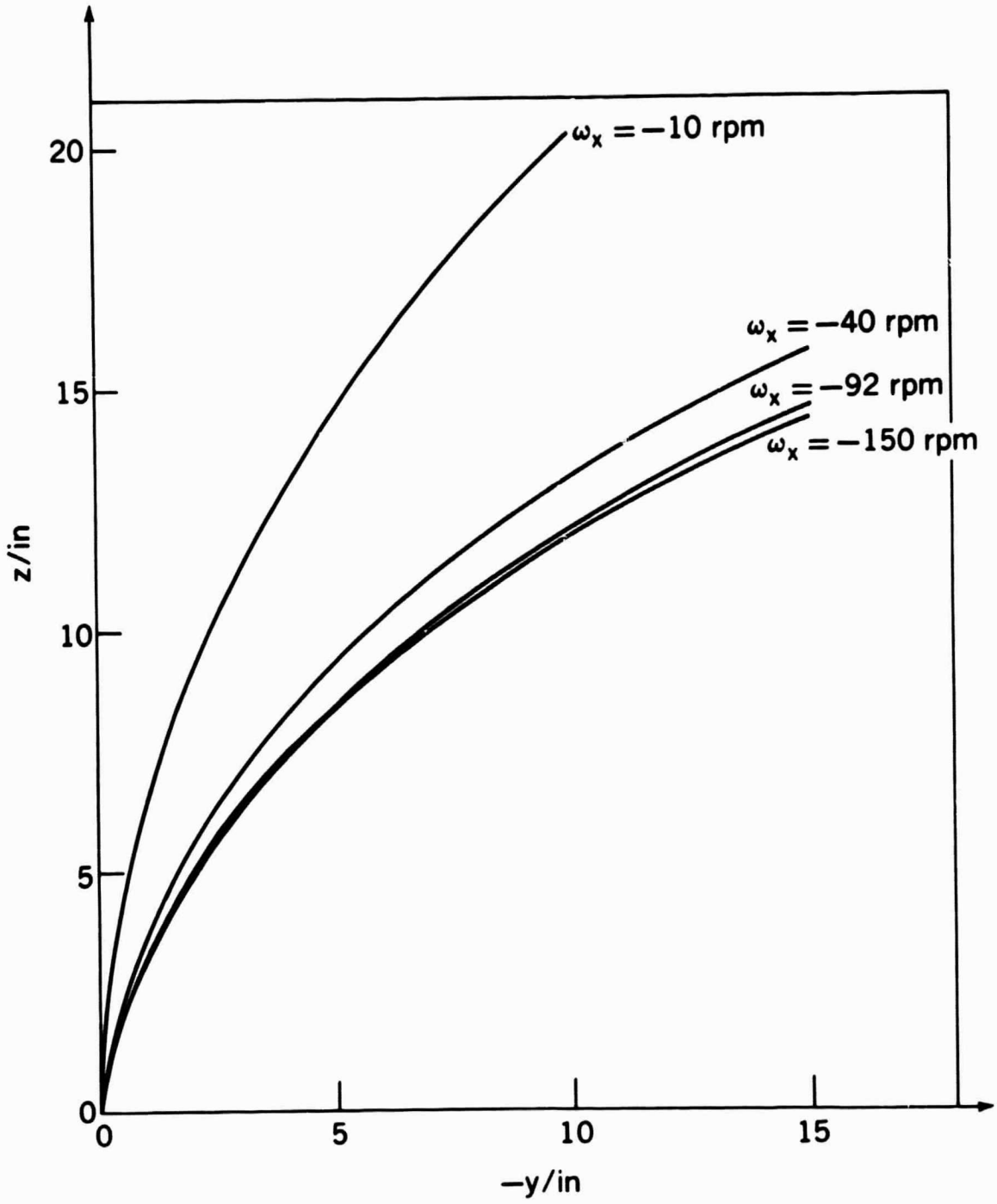

Figure 4. Trajectory of the apogee motor relative to the main spacecraft after deployment by a spring, at different values of ω_x.

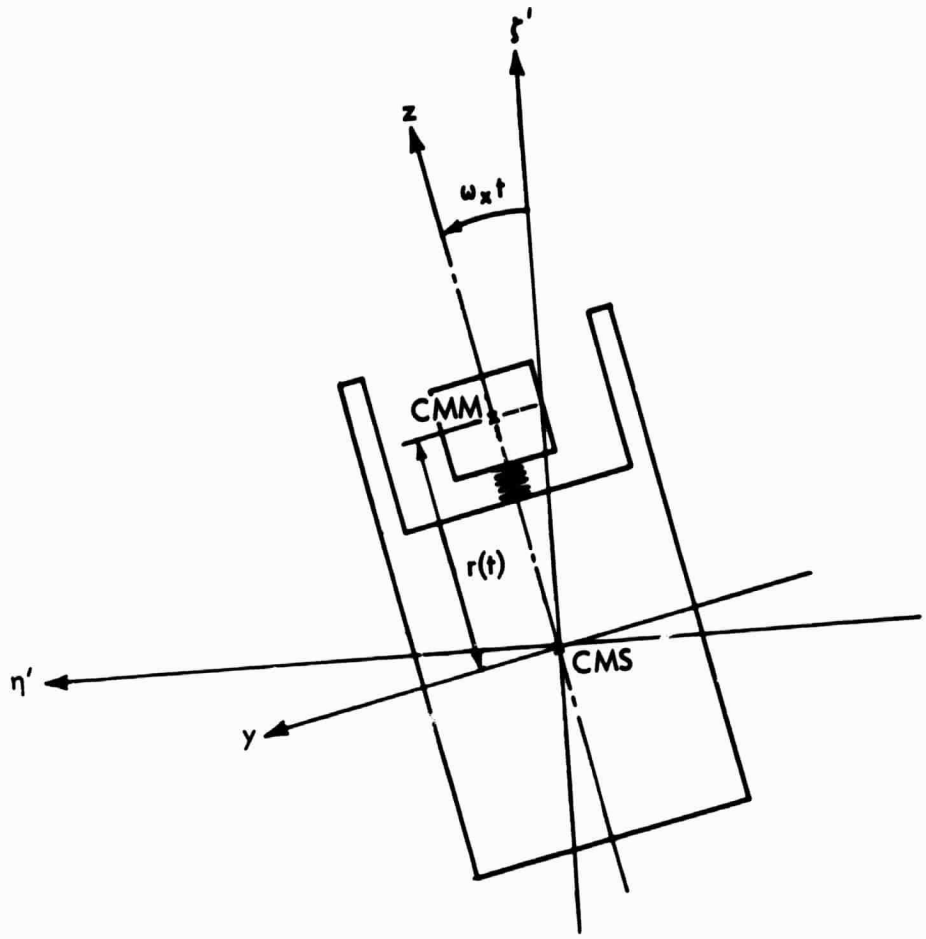

Figure 5. Release mechanism model – time dependent acceleration.

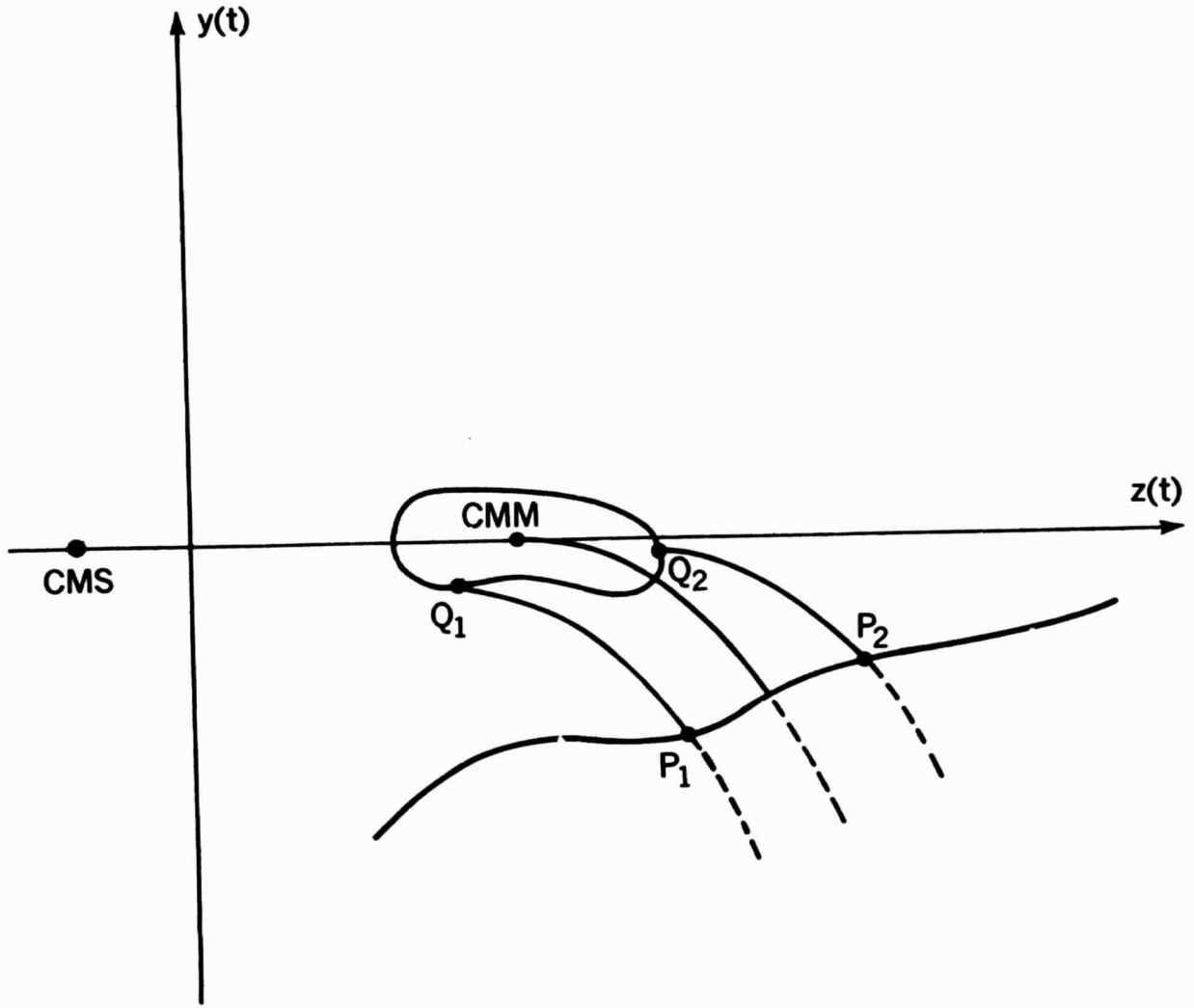

Figure 6. Collision point mapping.

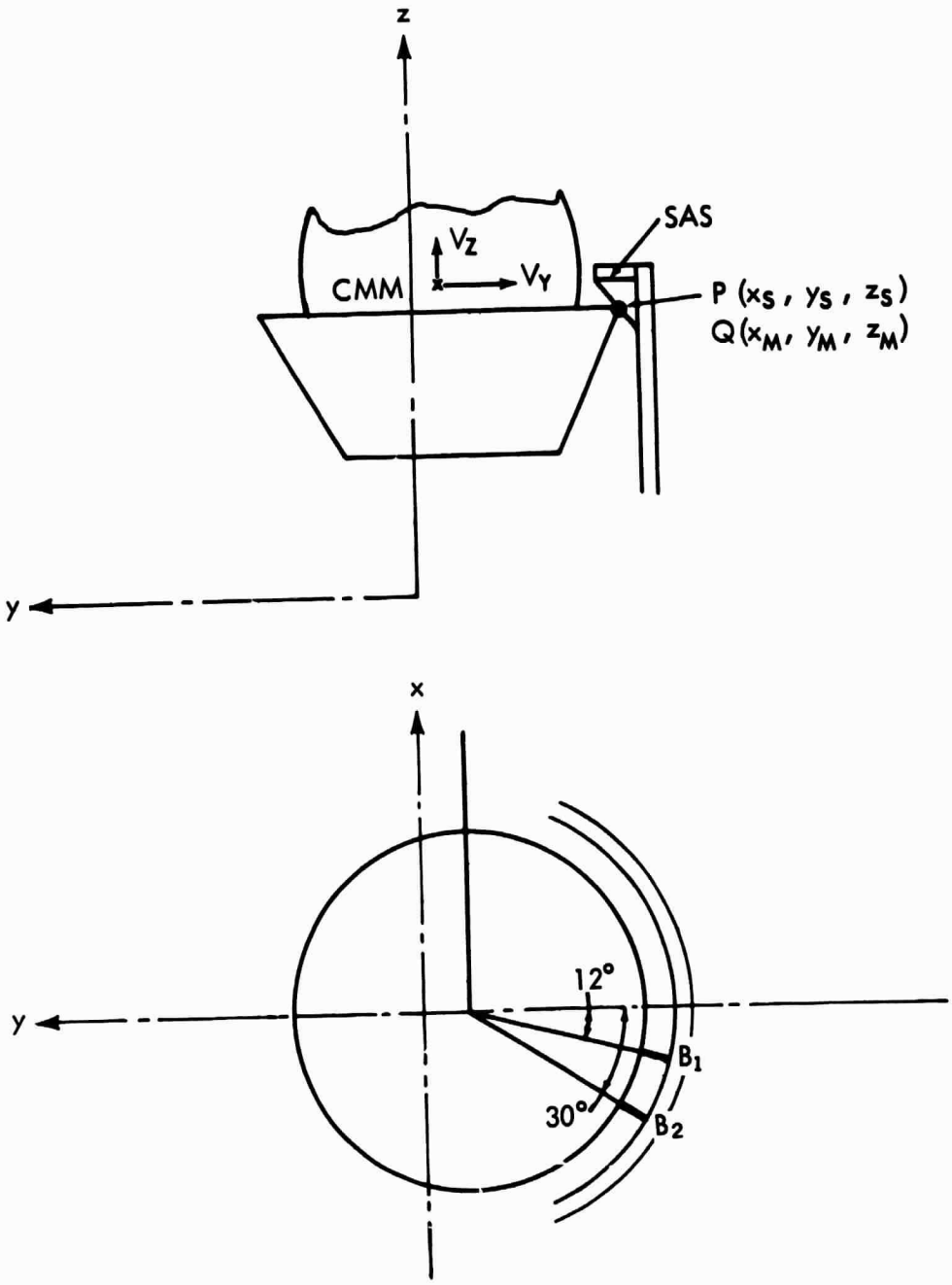

Figure 7. Collision point and surrounding area.

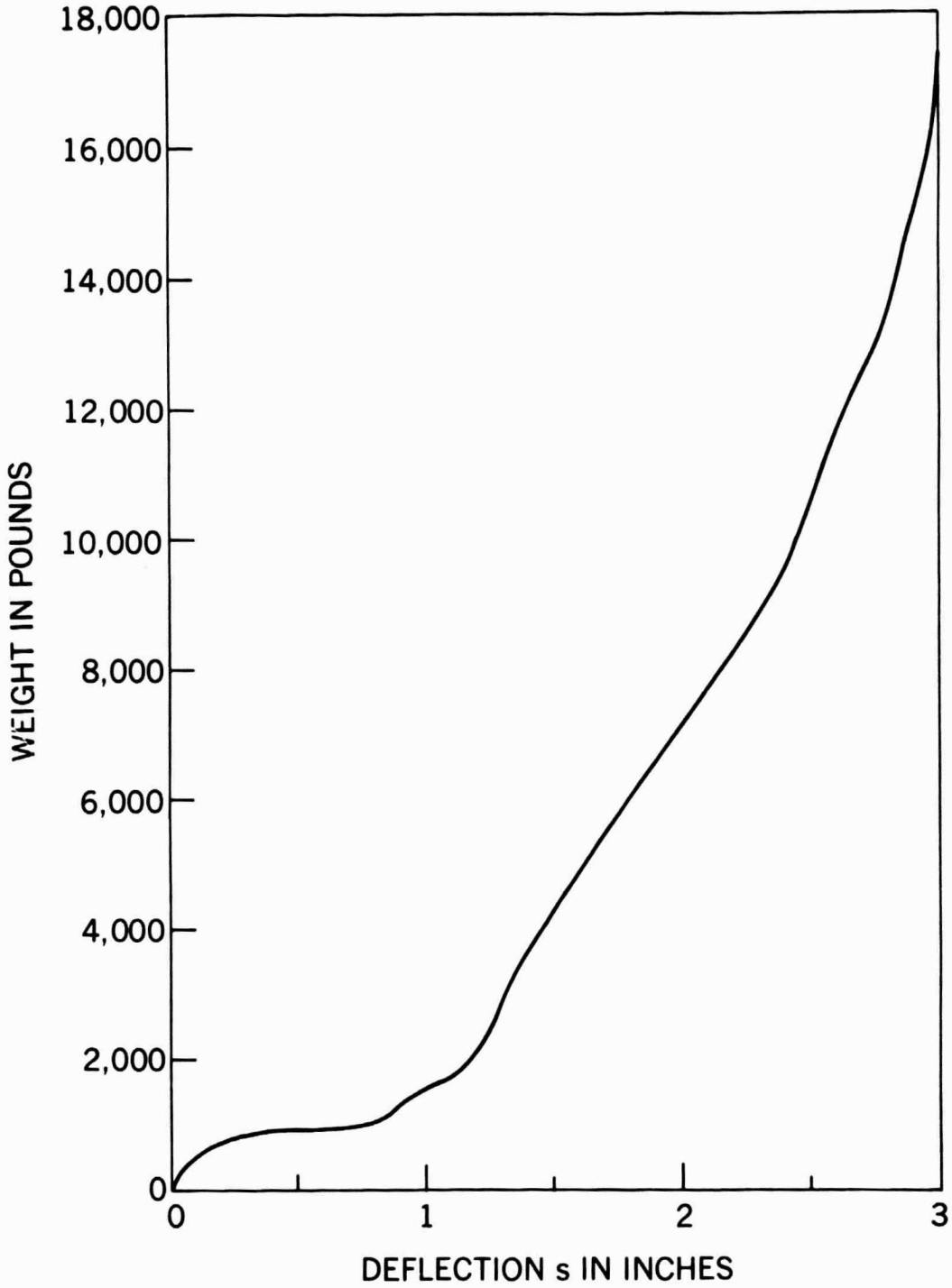

Figure 8. Static load test for deformation of both brackets B_1 and B_2, both starting being deformed at the same time.

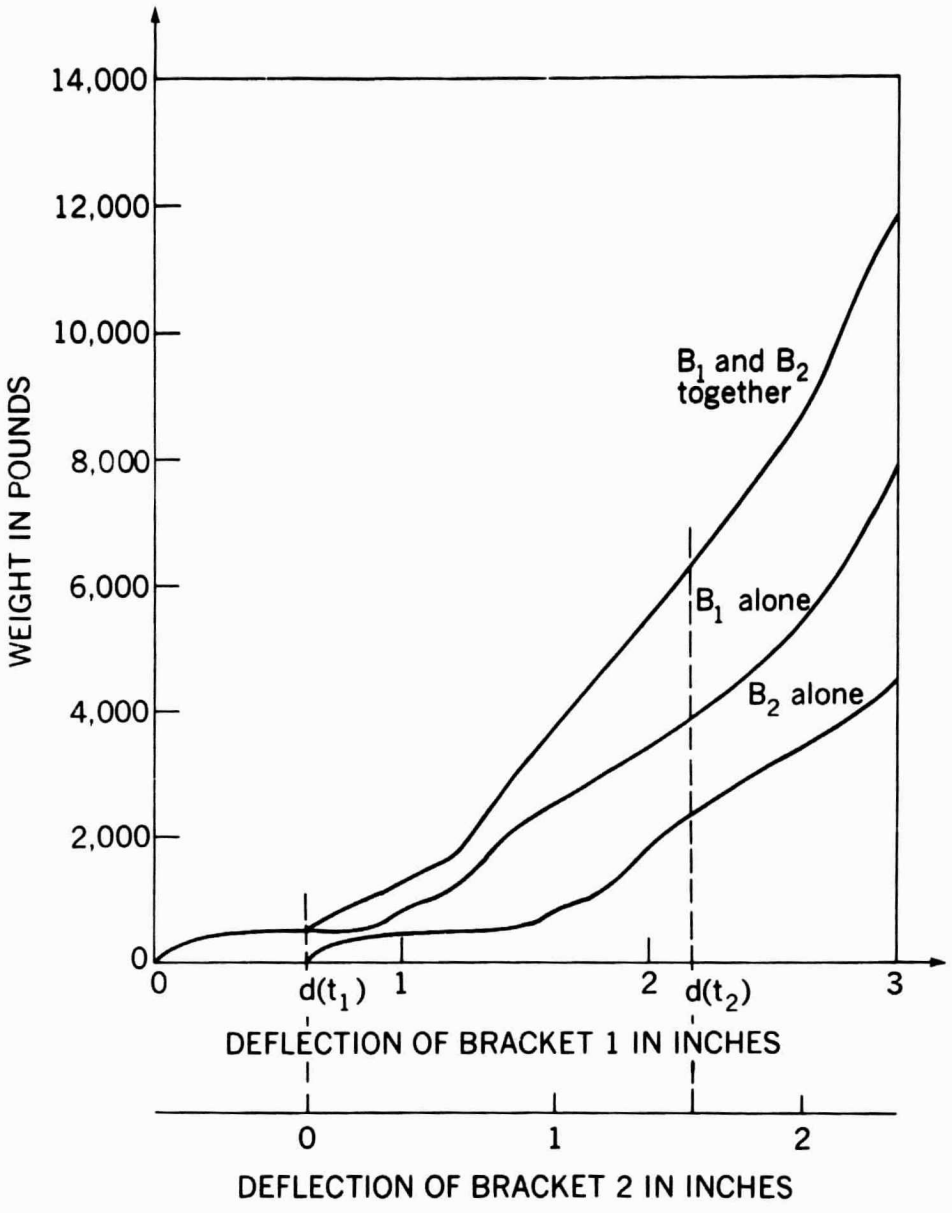

Figure 9. Static load versus actual deformation of the two brackets.

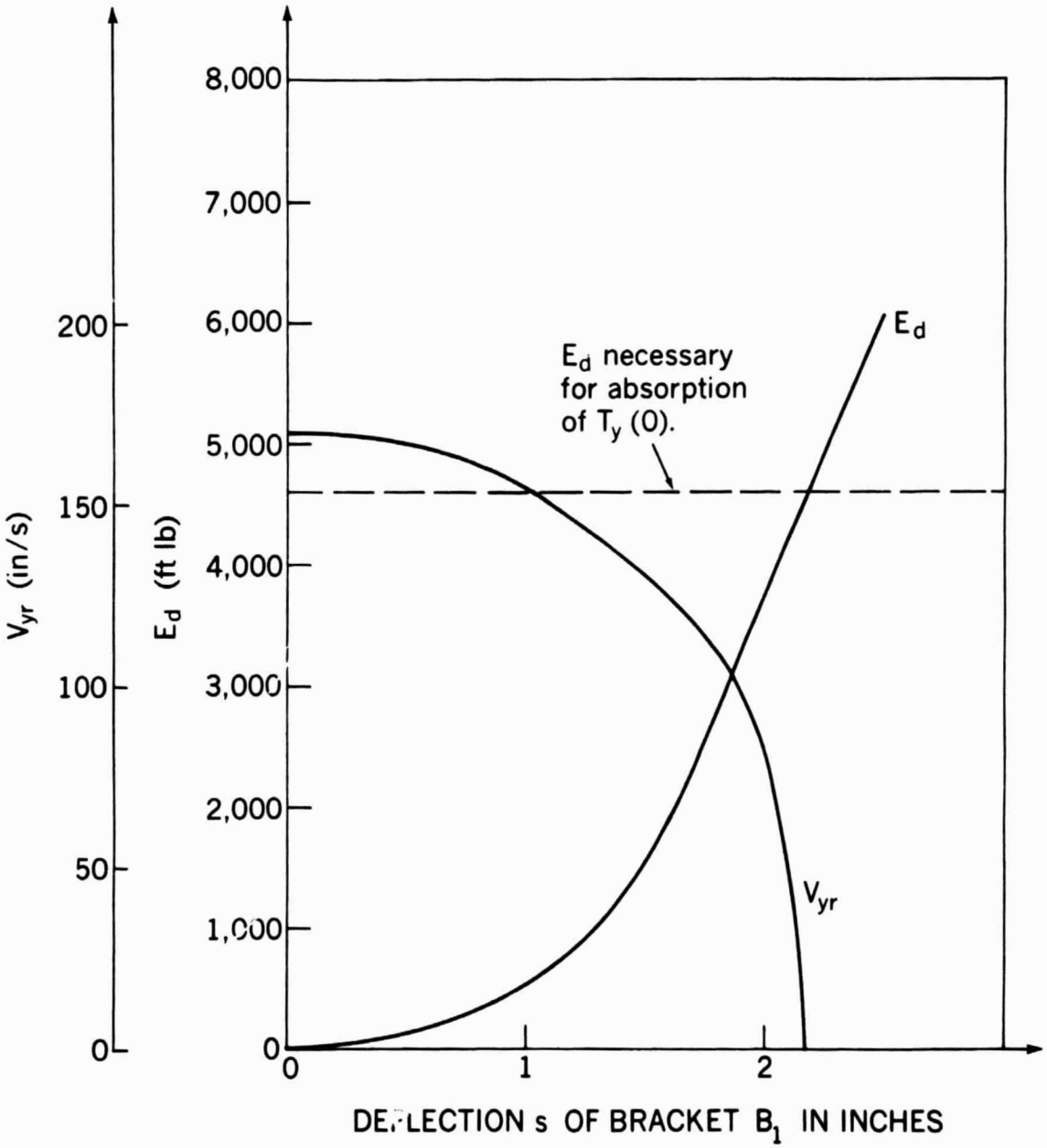

Figure 10. Closing velocity of internal mass and energy stored in the deformed structure versus deflection s.

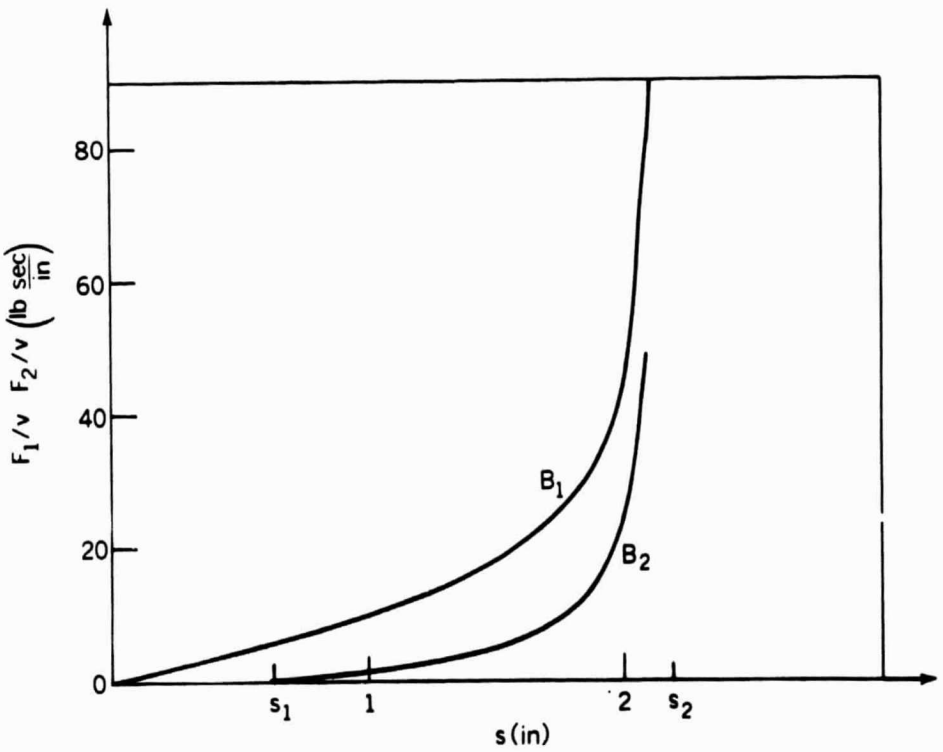

Figure 11. Ratio of F_i (i = 1, 2) and closing velocity versus deflection s for calculation of the collision vector $\vec{S}$.

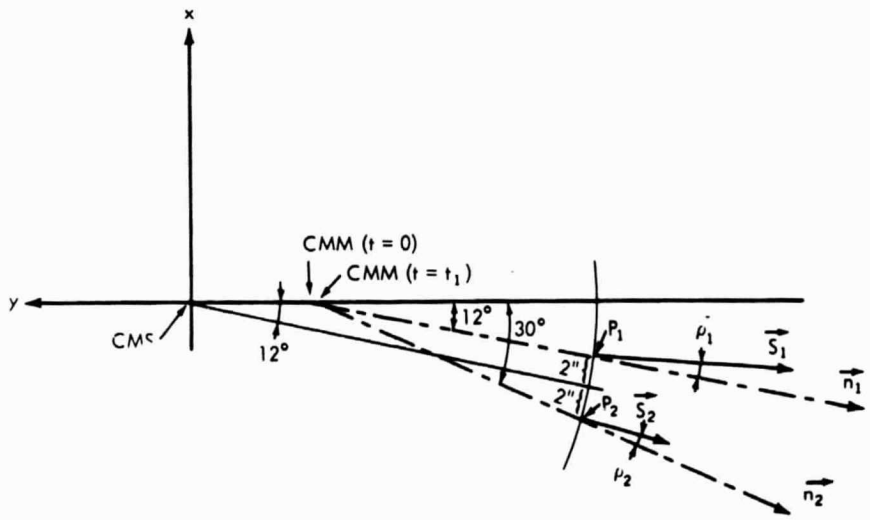

Figure 12. Configuration of CMS, CMM, $\vec{S}_1$ and $\vec{S}_2$ during collision
P_1 point of collision on bracket B_1
P_2 point of collision on bracket B_2
$\rho_1 = \rho_2$ for $\rho_1 \leq 12°$

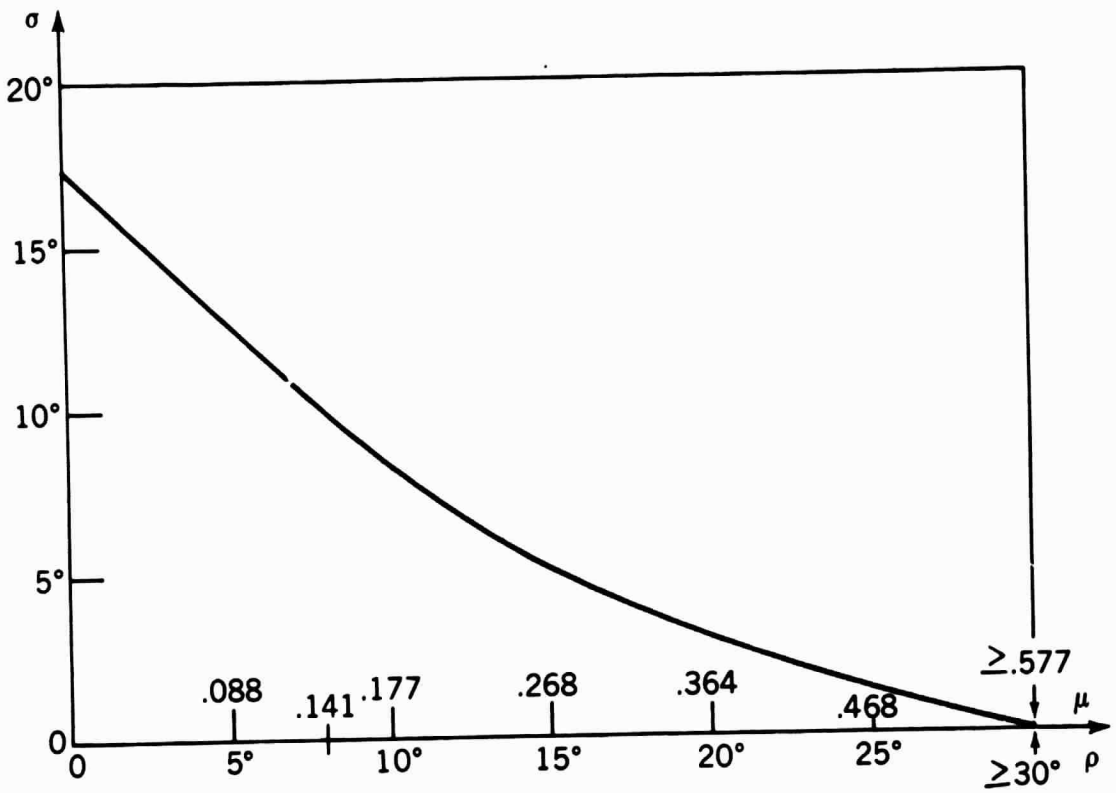

Figure 13. Angle σ of equivalent collision vector S against negative y-axis compared with ρ for $\vec{S}_1$ and $\vec{S}_2$.

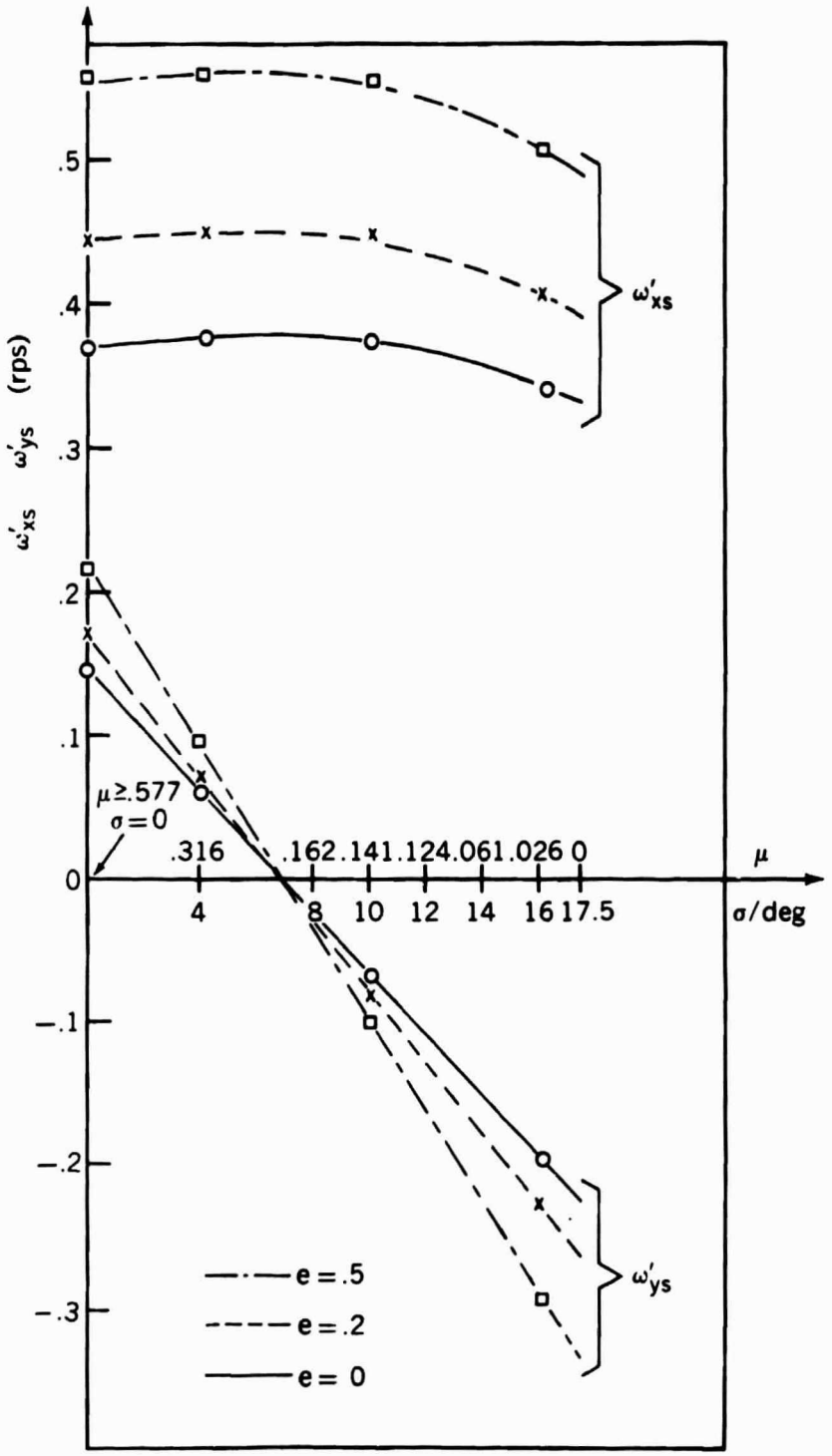

Figure 14a. Changes of ω_x and ω_y as a function of σ (and therefore as a function of μ according to Fig. 12). The parameter is the coefficient of restitution which gives the degree of elasticity involved.

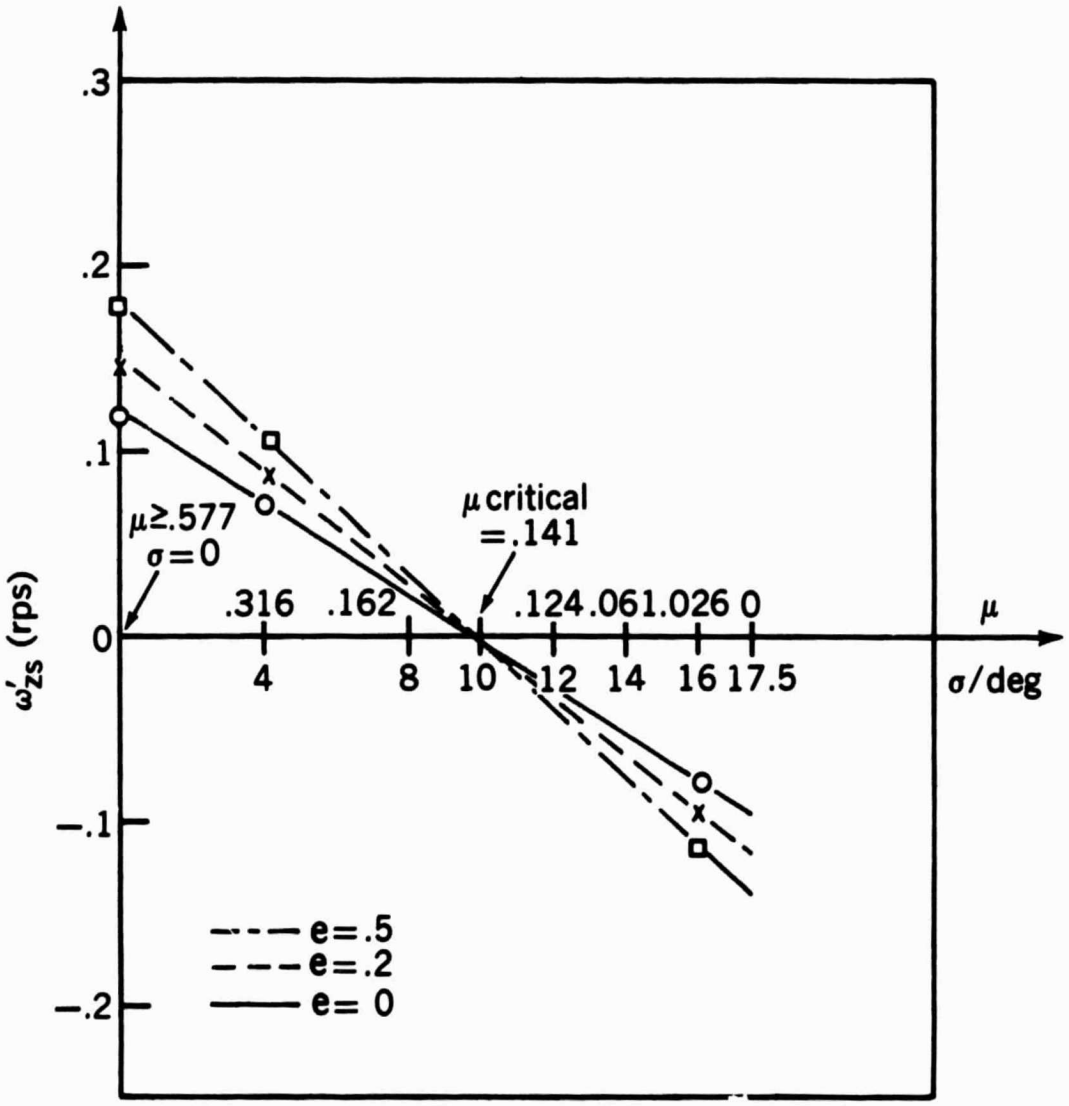

Figure 14b. Changes of ω_z as a function of σ (and therefore as a function of μ according to Fig. 12). The parameter is the coefficient of restitution which gives the degree of elasticity involved.